Sociedad Mexicana de Ingeniería Mecánica
Fecha de recepción: 15-11-2012
Fecha de aceptación: 25-02-2012

INGENIERÍA MECÁNICA
TECNOLOGÍA Y DESARROLLO
Vol. 4 No. 2 (2012) 061 - 071

Two-Phase Flow through the Drainage of a Porous Hele-Shaw Cell

Luviano-Ortiz J. Luis[1], Ramos Eduardo[3], Hernández-Guerrero Abel[2], Hernández-Cruz Guillermo[3]
[1]Instituto Tecnológico Sanmiguelense de Estudios Superiores
San Miguel de Allende, Guanajuato., México
[2]Mechanical Engineering Department,
University of Guanajuato, Salamanca, Guanajuato., México.
[3]Center of Energy Research, Universidad Nacional Autónoma de México
Temixco, Morelos, México.
luisluviano@gmail.com; erm@cie.unam.mx; abel@ugto.mx, ghc@cie.unam.mx

Resumen

En este trabajo se presenta el estudio experimental de un flujo bifásico de agua-aire dentro de una celda de Hele-Shaw rectangular de 19 cm × 41 cm × 1 mm; la celda se encuentra saturada con esferas de vidrio esféricas de 1 mm de diámetro. El flujo se caracteriza mediante la refracción de la luz en el menisco de la interfaz agua-aire como un indicador para determinar la posición de la interfaz en función del tiempo. El movimiento del líquido se genera llenando parcialmente la celda con agua y permitiendo después que esta salga a través de un orificio ubicado en la parte inferior de la celda. Se observa que, en contraste con lo que ocurre en una celda de Hele-Shaw sin esferas, la interfaz líquido-aire es una línea irregular con movimientos repentinos localizados, generados por los efectos de la tensión superficial que se produce debido a los arreglos desordenados de las esferas. Estas observaciones son potencialmente útiles en la extracción de petróleo y en la caracterización de los flujos de agua subterránea.

Abstract

This work presents an experimental study of liquid-air flow inside a 19 cm × 41 cm × 1 mm rectangular Hele-Shaw cell, saturated with 1 mm diameter spherical glass beads. The flow is characterized by using light refraction at the liquid-gas interface menisci as a marker to determine the time-dependent position of the liquid-gas interface. In the experiment liquid motion is generated by partially filling the cell with water and then letting the water out through an outlet in the lower part of the cell. It has been observed that, in contrast to what occurs in a Hele-Shaw cell with no spheres, the liquid-gas interface is an irregular line that moves with localized sudden motions generated by surface tension effects occurring due to the non-regular arrangements of the spheres. These observations are potentially useful in the petroleum extraction and underground water flows.

Palabras clave:
Desagüe, celda de Hele-Shaw, cuentas de vidrio, retención de agua, desagüe por gravedad

Keywords:
Drainage, Hele-Shaw cell, glass beads, water retention, forced gravity drainage

Nomenclature

D	Diameter
n	Porosity
y	vertical coordinate
t	Time
T	Normalized time
DF	Fractal dimension
C_{DN}	Normalized discrete compactness

INTRODUCTION

Two-phase flows in porous media appear in many important industrial and geological applications, such as oil recovery or ground water flow modeling, where an increase in the recovery rate is obtained by injection of another fluid phase [Bear (1972), Homsy (1987) and Tchelepi and Orr (1994)]. For immiscible flows, a wide range of behaviors are observed depending on the wetting properties of the two fluids, their viscosity ratio, their respective density, and the displacement rate [Avraam and Payatakes (1995) Lenormand & Zarcone, (1985)].

Gas injection has been considered as a very attractive oil recovery process especially when it is assisted by gravity drainage. For immiscible flows, the displacement efficiency could depend on the wetting properties of the fluids, the rate of gas injection and the oil production, the difference of oil and gas density, their viscosity ratio, and the oil relative permeability. Experimental investigations, both in the laboratories and in the field [Da Sle and Guo (1990) and Hagoort (1980)] suggest the importance of the gas–oil gravity drainage process in improving the recovery characteristics of gas injection EOR (experimental oil recovery) methods.

The morphology of the displacement structures observed in immiscible two phase flow is in general controlled by the competition between viscous forces, gravitational forces and capillary forces; those various forces act on scales ranging from the pore scale to the system size. The relative wettabilities, viscosities and densities of the fluids, as well as the heterogeneity of the underlying porous media, could all play important roles in the competition process [Homsy (1987),

Måløy, Feder and Jøssang (1985), Birovljev, Furuberg, Feder, Jøssang, Måløy and Aharony (1991), Måløy, Furuberg, Feder and Jøssang (1992) and Frette, Maløy and Schmittbuhl, (1997)].

If one considers situations in which a non-wetting fluid invades a porous medium saturated with a wetting fluid (drainage) with a higher viscosity, in the absence of gravity, two regimes can be distinguished. At very low flow rates, the viscous pressure drop across the porous medium is negligible in comparison to the inhomogeneity in the threshold capillary pressures inside the medium. The topology of the random porous medium causes the fluctuations in the pressure field needed for the non-wetting phase to invade new pores. The resulting displacement structure is controlled by capillary effects, and it is well described by the invasion percolation algorithm. This capillary fingering regime has been studied extensively [Lenormand & Zarcone (1985) and Lenormand and Zarcone (1989)]. At high flow rates, viscous forces dominate capillary and gravitational effects. The displacement is stable or unstable depending on which phase is the most viscous [Homsy, (1987), Måløy, Feder and Jøssang (1985), Frette, Maløy and Schmittbuhl (1997) and Aker, Måløy and Hansen (2000)]. If the defending phase is the most viscous one, the displacement is unstable [Homsy, (1987), Måløy, Feder and Jøssang (1985), Chen and Wilkinson (1985) and Nittman (1986)]. This viscous fingering regime has strong analogies to diffusion-limited aggregation (DLA) patterns [Witten and Sander (1981), Witten and Sander (1983), Meakin (1983), Paterson (1984) and Hinrichsen, MåLøY, Feder and Jøssang (1989)]. For the opposite case in which the invading fluid is the most viscous one, viscous effects stabilize the front [Aker, Måløy and Hansen (2000) and Dullien (1988)].

However, most real reservoir systems are not flat and horizontal, and are therefore sensitive to gravity effects. If the two fluids involved have different densities, gravity forces modify the displacement structure dramatically [Birovljev, Furuberg, Feder, Jøssang, Måløy and Aharony (1991), Wilkinson (1984), Birovljev, Wagner, Meakin, Feder, and Jøssang (1995) and Wagner, Birovljev, Meakin, Feder, and Jøssang (1997)]. Gravity causes hydrostatic pressure gradients that might stabilize or destabilize fluid motion.

The competition between gravity and viscous forces has been studied for immiscible flows in a Hele-Shaw cell without any porous medium. Saffman and Taylor have studied small perturbations of the displacement front, deriving a criterion for the instability [Saffman and Taylor (1958)]; but it is not obvious that the arguments developed for this particular geometry apply to flows in porous media, where the complexity of the flow boundary conditions plays a crucial role [Chen and Wilkinson (1985)]. The deformation and breakup of non-wetting clusters by a viscous pressure field has also been studied for a system without gravity effects [Vedvik, Wagner, Oxaal, Feder, Meakin and Jøssang (1998)]. Situations where all three forces are significant have been studied for imbibition in a sand pack [Zhou and Orr (1995)], with a focus on the saturation of the non-wetting fluid, and for simulations of viscous fingering in a gravity field, at the reservoir scale [Tchelepi and Orr (1994)].

In the capillary fingering regime, stabilization of the fluid interface by gravity has been studied both theoretically and experimentally in two and three dimensional media [Birovljev, Furuberg, Feder, Jøssang, Måløy and Aharony (1991) and Wilkinson (1984)]. Unstable buoyancy driven migration of a lighter fluid into a denser one has also been studied by use of experiments, computer simulations and theoretically [Birovljev, Wagner, Meakin, Feder, and Jøssang (1995), Wagner, Birovljev, Meakin, Feder, and Jøssang (1997), Frette, Feder, Jøssang and Meakin (1992), Meakin, Birovljev, Frette, Feder and Jøssang (1992) and Wagner, Meakin, Feder and Jøssang (1997)]. All these studies of gravitational effects concentrate on situations where the flow rates are so low that capillary forces are large compared to viscous forces at pore scale. For such systems the obtained flow patterns are understood in terms of the competition between gravity forces and local non-homogeneous capillary forces [Birovljev, Furuberg, Feder, Jøssang, Måløy and Aharony (1991) and Wilkinson (1984)]. It should be noted that although the obtained displacement patterns could be modeled without considering viscosity, viscous effects have to be taken into account to understand the local dynamics during invasion [Haines (1930)].

The purpose of this work is to present the results found for a drainage experiment in which non-wetting air displaces the wetting distilled water in a vertical two-dimensional porous medium; hence, gravity has influence on the displacement. The porous medium consists of a Hele-Shaw cell filled with a random monolayer of monodisperse spherical glass beads. In this paper, the regime of slow displacement for which capillary forces control the dynamics of the invasion process and the geometry of the resulting invasion structure (capillary fingering), is studied; the fast displacement where viscous forces are dominant (viscous fingering) is analyzed as well.

EXPERIMENTAL SET-UP

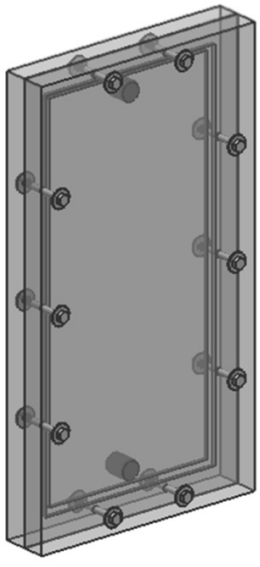

Figure 1.Schematic representation of the Hele-Shaw cell.

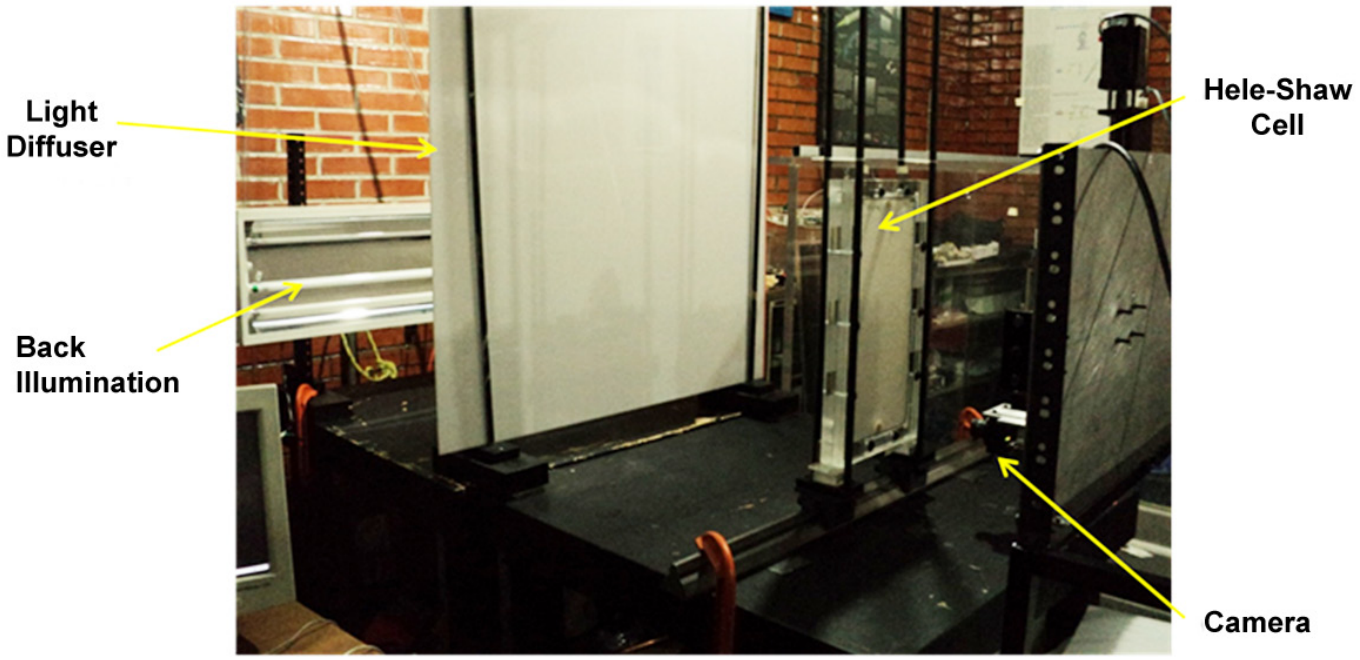

Figure 2. Experimental set-up.

The experiments were performed on a quasi two-dimensional porous medium of dimensions 19 cm × 41 cm × 1 mm, contained in a Hele-Shaw cell (Figure 1). The construction of the cell was carried out by using two transparent acrylic plates (Plexiglas brand) of 25.5 cm × 47 cm × 2.5 cm, with a 1 mm gap. In order to introduce and remove fluid from the cell, two boreholes of ½" in diameter were made on one of the acrylic plates. The porous medium was prepared using a random mono layer of glass beads. On the periphery of the plate with the two boreholes an O-ring (Parker brand) of 1/16" in diameter was stuck; this O-ring was used as packing, therefore, the cell was sealed off at the edges, forming a rectangular porous medium.

To prevent that the glass beads escape through the fluid inlet and outlet (½" boreholes), a filter, acting as a seal, was positioned. This filter is of the type currently used in domestic faucets to avoid particles. In the spacing between the plates, and next to the screws, stainless steel shims (Precision Brand, hardness Rockwell C40-45) of thickness 1 mm were placed. This also served to make sure that the internal spacing of the cell was 1 mm. The experimental set-up of the equipment used in the laboratory experiments is shown in Figure 2.

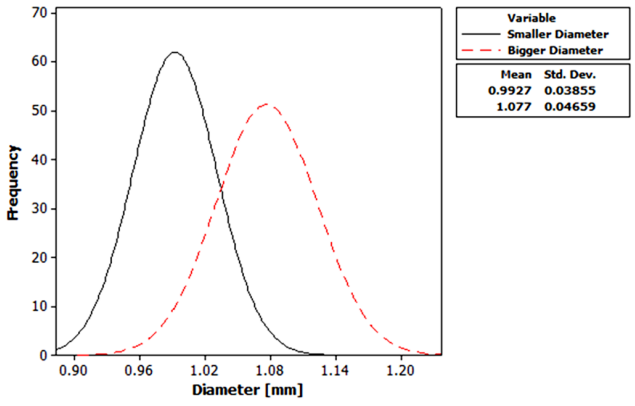

Figure 3. Histograms of the bigger and smaller diameters of the glass beads.

Grain Size

Due to the fact the porous medium consists of spherical glass beads, the porous medium needed to be characterized in order to be able to determine its different properties. First of all, it was necessary to determine the grain size; to accomplish this, the diameters of the spheres were measured and it was found that the spheres have actually an ovoidal shape (having thus two main diameters). Figure 3 shows the diameter size obtained by measuring 300 glass beads. The statistical values (mean and standard deviation) of the main diameters are shown in the upper right box of the figure.

CHARACTERIZATION OF THE POROUS MEDIUM

Estimation of the Number of Spheres Contained in the Porous Medium

In order to determine the total amount of spheres contained in the porous medium, the cell was sectioned into different rectangular areas and the photographs of each of these areas were taken. Once the photographs of all the areas were obtained the pictures were joined in such a way that a single photograph representing the whole porous medium was obtained; subsequently the Hough Transform Method was applied to this picture. Once the algorithm of the Hough Transform was applied to the photograph of the whole porous medium, the total number of spheres contained in the Hele-Shaw cell was determined; the number of spheres calculated for the whole porous medium was 74576.

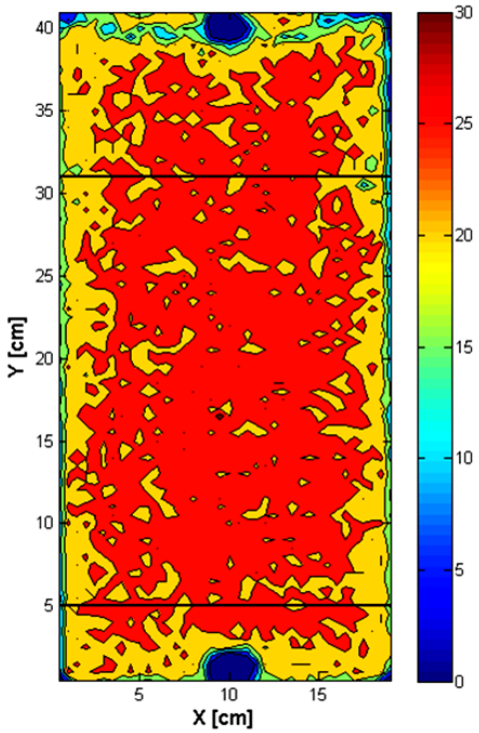

Figure 4. Density map of the glass beads distributed in the Hele-Shaw cell. Color code = number of spheres per 25 mm^2.

Density Map of the Porous Medium

Figure 4 shows the density map of the distributed spheres in the Hele-Shaw cell. In this figure it is observed that most of the spheres are placed in the central region of the cell, while fewer spheres are close to the walls of the cell. The two bigger areas in blue correspond to the fluid input and output; in these regions the filters that prevent the spillage of the spheres are placed, making it hard to illuminate these areas to estimate the number of spheres there. Nevertheless, this does not affect the estimates of the experiments since the area in which the experimentation was carried out was the region between the two black horizontal lines (5 cm $\leq y \leq$ 31 cm) of Figure 4.

Porosity Map of the Porous Medium

Figure 5 shows the map corresponding to the porosity of the porous medium; the sphere diameter that was used to obtain this map was the average of the means corresponding to the bigger and smaller diameters of the spheres of Figure 3 (D = 1.0348 mm). As it was pointed out above, it was not possible to determine the number of spheres for the inlet and outlet zones, therefore, the porosity value in these regions was set to $n = 1$.

OBSERVATIONS OF THE DYNAMICS OF THE INTERFACE FOR A SLOW FLOW IN A PARTIALLY FILLED CELL

Due to the fact that the experiments consist in draining the Hele-Shaw cell, which is partially full of distilled water, it is essential to know the evolution of the interface water-air. To accomplish this, several experiments were carried out for which the cell was filled with distilled water to a height of y = 31 cm; the filling of the cell proceeded slowly in order to have an initial interface as uniform as possible and the water filling was done through the lower hole of the cell.

In order to obtain a slow flow, the valve at the outlet of the cell was regulated in such a way that the time of draining from the position y = 31 cm to the position y = 5 cm (measured from the bottom of the cell) was about 20 minutes to obtain a flow rate of about 127 ml/h. The reason for displaying the interface change between the positions 5 cm $\leq y \leq$ 31 cm is with the aim

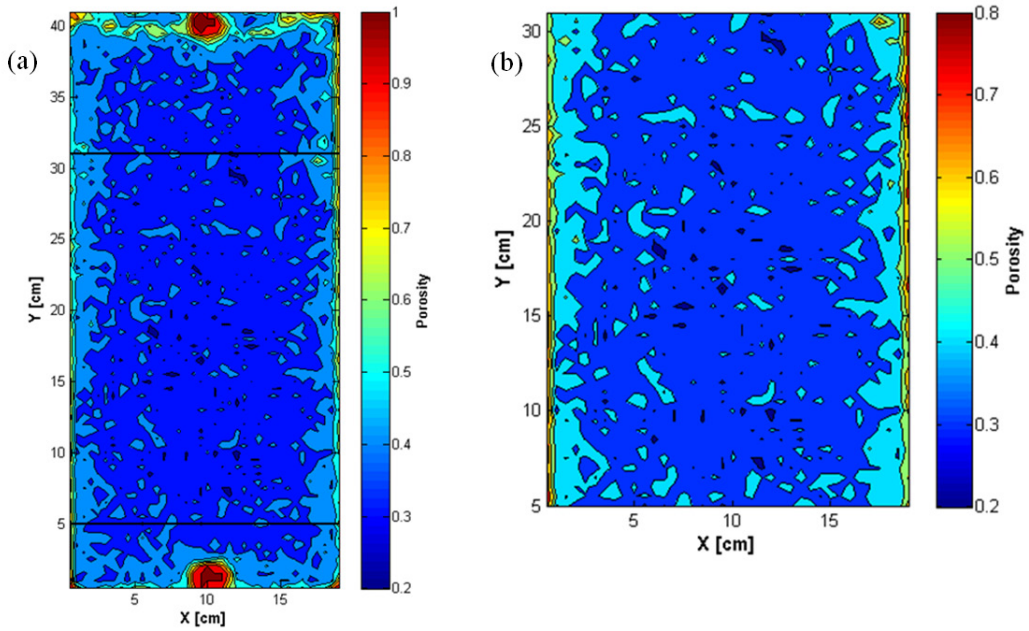

Figure 5. Porosity map of the porous medium. (a) Porosity of the whole cell, (b) porosity of the visualization area (area between the black horizontal lines of Figure 5 (a).
Color code = porosity per 25 mm^2.

of using the highest resolution of the BASLER camera, that is, it is the maximum height of the cell that can be captured when the entire width of the cell is visualized.

Since the spacing between the plates is small (≈ 1 mm), it is considered that the system is quasi-two-dimensional. The images for the slow flow were taken with a spatial resolution of 0.32 mm per pixel and 256 gray scale levels per pixel. The interval between each image was 100 ms (10 fps). The background was the same for all the images captured with the same camera, therefore the interface was enhanced by subtracting the first image to all other images, and thresholding the result to get a black and white contour of the interface. The contour was fixed to a 1-pixel accuracy using edge detection methods, and data stored for further analysis; in order to process this image a program in MATLAB was written.

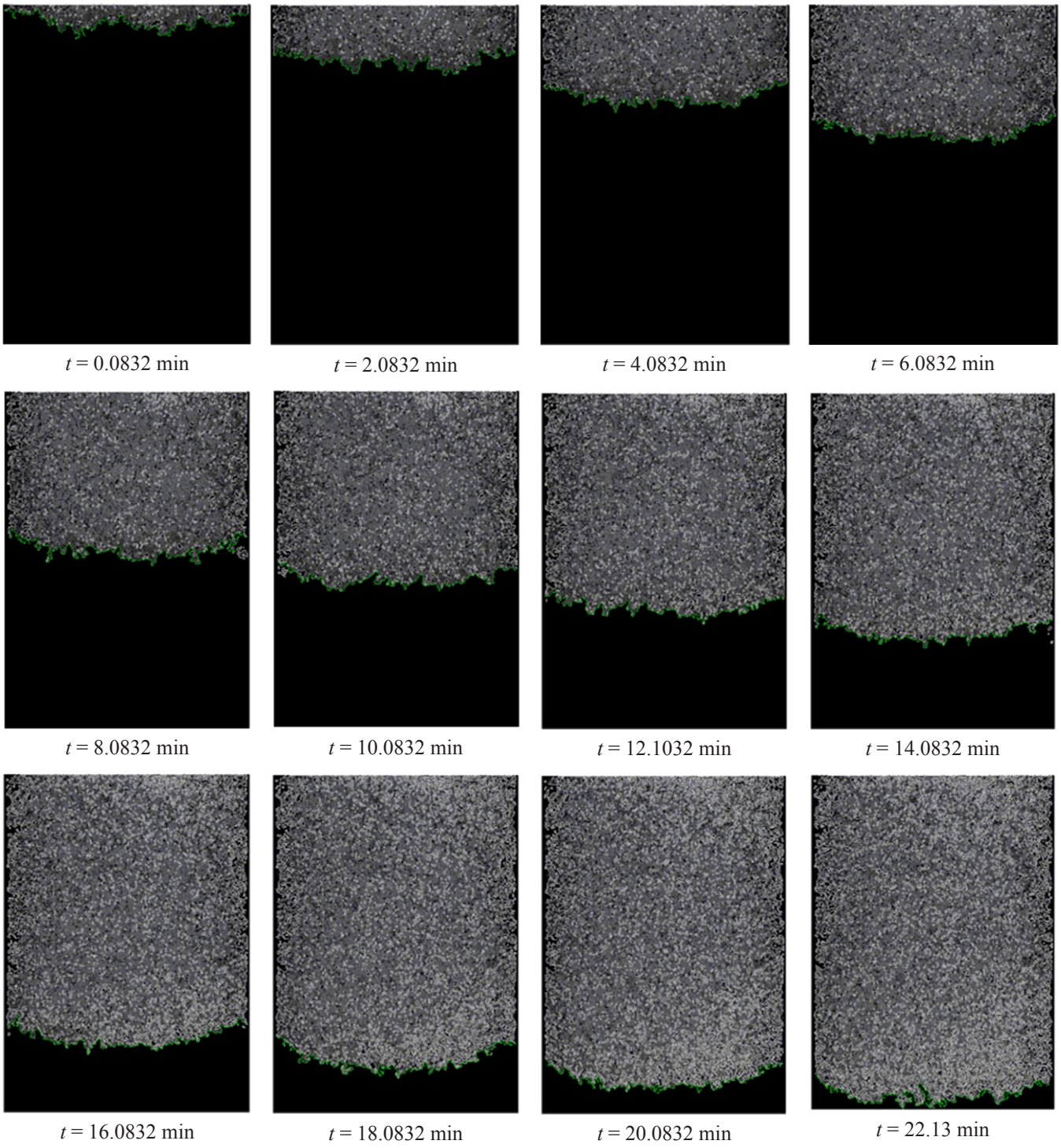

Figure 6. Profile of the interface for the slow flow during the drainage of the cell.

Figure 6 presents the sequence of several processed images (where the interface has been enhanced). This sequence allows the observation of the time evolution of the interface air-water while the cell is being drained. The interface clearly shows a corrugated shape throughout the drainage; it is also observed that around the central part of the interface the water flows faster even though the medium is less porous in that region (Figure 5). In this figure it can also be appreciated that in the areas located above the interface there are small "black islands" representing trapped water or water that is falling more slowly, indicating therefore that not all the water is removed in the drainage. Later on, a fraction of the water that was trapped in some of the islands breaks off and reaches the main flow (black area), modifying thus the length of the interface.

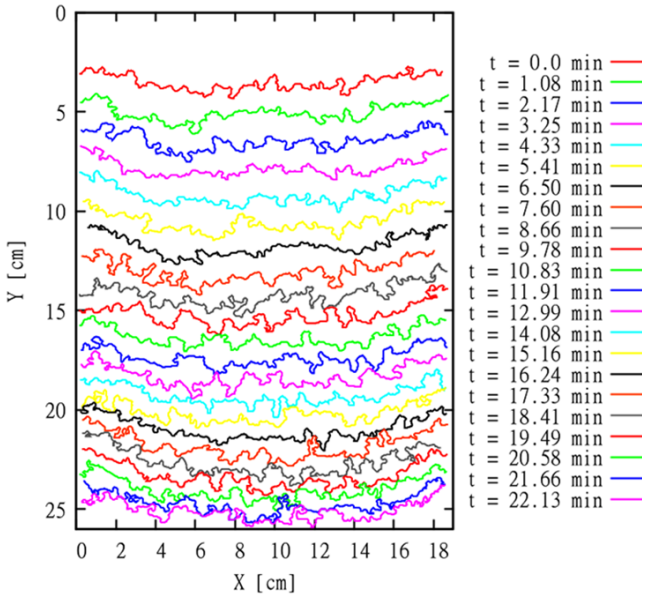

Figure 7. Interface sequence of the slow flow for different times of drainage.

In order to present the results in a clear way, the origin of the coordinate system is located at the upper right corner of the visualization window (region between the horizontal black lines in Figure 4). Figure 7 shows the interface water-air for different times of the drainage. The drainage of the cell starts from the top horizontal axis of the visualization window, however, given the physical conditions of the phenomenon, the total length of the interface can be captured from the position shown in Figure 7; it is from this position that the time of drainage is measured. The drainage time for the slow flow was t = 22.13 min. This figure allows following the evolution of the interface as well as its corrugation; likewise, it can be observed that the interface in some regions has two values of Y for a single value of X, (this implies that the curve of the interface is not a mathematical function).

Length of the Front as a Function of Normalized Time

Figure 8 shows the normalized length of the interface (interface length/cell width) as a function of normalized time; in the upper left box the total time of the drainage is displayed: t = 22.13 min. The time increment between each plotted point is Δt = 0.1 s. In this figure it is possible to appreciate that the

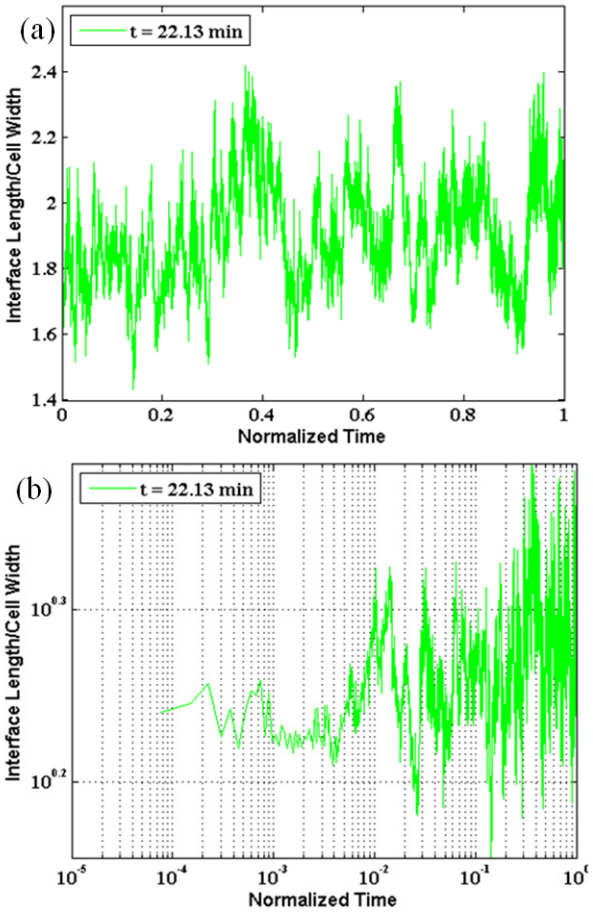

Figure 8. Normalized length of the interface as a function of normalized time for the slow flow. (a) Cartesian coordinates, and (b) log-log coordinates.

normalized length of the interface ranges from 1.4 to 2.4, that is, the smallest length of the interface is 1.4 times larger than the cell width, while the biggest length of the interface is 2.4 times larger than the width of the cell.

Fractal Dimension

With the aim of determining the interface corrugation, the theory of fractal media was used, with the aid of the FRACTALYSE software (Version 2.4); and the method used to calculate the fractal dimension was *Box Counting*. The fractal dimension of the slow flow with respect to normalized time is shown in Figure 9. In this figure it is possible to observe that the fractal dimension (FD) ranges between the values 1.015 $\leq FD \leq$ 1.135, therefore, it is possible to state that the fractal dimension of the slow flow is $FD = 1.075 \pm 0.06$.

Bribiesca's Discrete Compactness for Slow Flow

The interfacial lines can be parametrized using the Bribiesca compacity or discrete compactness. See Bribiesca [Bribiesca (1997)]. Before describing this concept, it is important to remark that the interfacial lines are defined by sequences of straight line segments of lengths equal or larger than the side of a pixel and oriented at 0, +/- 90 deg. with respect to the previous segment. An area limited by such a line, is composed by adjacent square elementary cells. The discrete com-

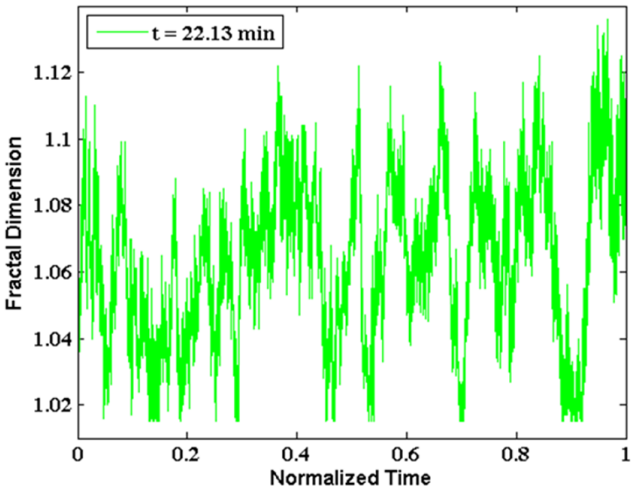

Figure 9. Fractal dimension with respect to normalized time for the slow flow interface.

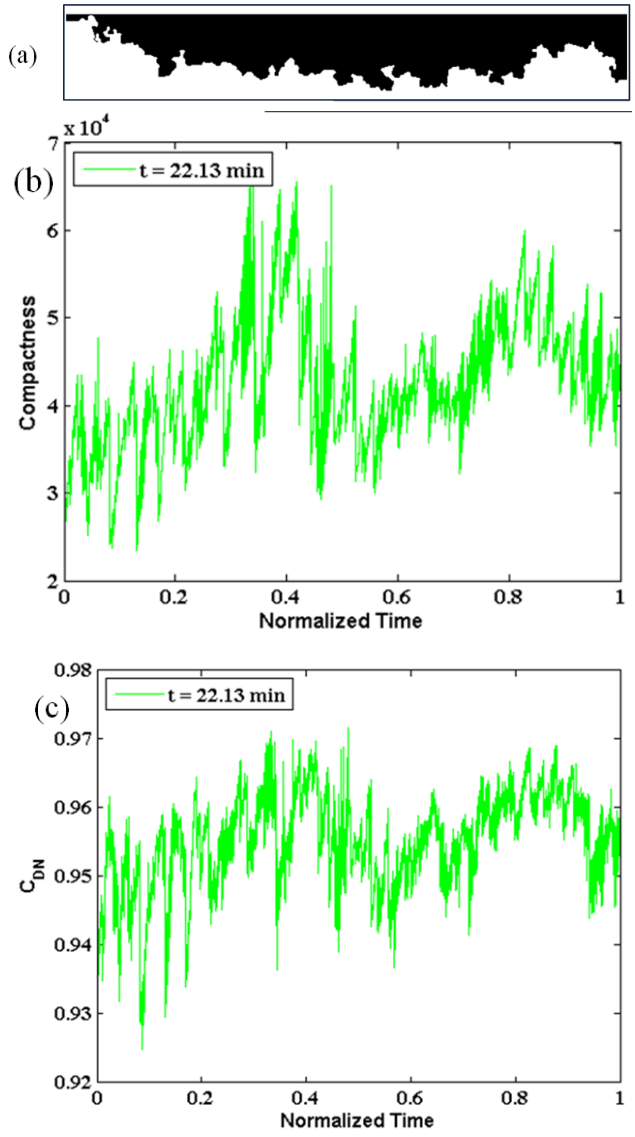

Figure 10. Discrete compactness using the contact perimeter. (a) Interface width of air (black area) on which the discrete compactness was calculated, (b) discrete compactness with regards to normalized time, (c) normalized discrete compactness C_{DN} with regards to normalized time.

pactness of an area enclosed by a boundary composed by straight line segments is defined as the sum of the boundaries of neighboring cells in the area. An interfacial line and three straight sides enclose an area and since the straight sides do not alter the compacity measure, the discrete compactness of the area can be used to characterize the interfacial line.

The concept of discrete compactness was applied to the black area of Figure 10 (a). In this area there is mainly air. To apply Bribiesca´s method, it was determined that the lower limit of the region to analyze should be the smaller value of the interface, and that the upper limit of this region should be the larger value of the interface. Once the regions to analyze were obtained, the Bribiesca method was applied, implementing a MATLAB code. Figures 10(b) and 10(c) show the discrete compactness and normalized discrete compactness, respectively.

Since the obtained discrete compactness of the interface is closely linked to its width, the increments and decrements in Figure 10(b) are equivalent to how the width of the interface is varying. This figure also shows that the discrete compactness of the interface increases and decreases gradually, however, the discrete compactness increases spontaneously at certain times; these increases are due to the fact that in a given time a fraction of the water that had been trapped in the islands mentioned above breaks off and reaches the interface, causing a wider interface. Figure 10(c) shows the variation of the normalized discrete compactness with respect to normalized time; this normalized discrete compactness can be interpreted as a factor indicating the similarity between the interfaces. In this figure it is possible to observe that the variation of the normalized discrete compactness is $0.925 \leq C_{DN} \leq 0.971$.

OBSERVATIONS OF THE DYNAMICS OF THE INTERFACE FOR A FAST FLOW IN A PARTIALLY FILLED CELL

The fast drainage of the cell is obtained by suddenly opening the valve located at the exit of the cell. As for the slow flow case, the cell was filled slowly with water through its bottom orifice up to a height of 31 cm (measured from the bottom of the cell).The area of the cell that was analyzed was the same as that of the slow flow. The images for the fast flow were taken with the same spatial resolution as those for the slow flow and the interval between each image was $\Delta t = 100$ ms (10 fps).

Figure 11 presents the sequence of several processed images for the fast flow; this sequence allows observing the time evolution of the interface, while the cell is drained. In these images it is observed that the interface is very different from the interface of the slow flow; it is also observed that the interfaces of the fast flow are more corrugated than the interfaces of the slow flow. As for the slow-flow case, in this figure also it can be appreciated that in the areas located above the interface there are also "small black islands" representing trapped water or water that is falling more slowly. Figure 12 shows the curves of the interface for different times of the fast flow drainage; the drainage time for the fast flow showed in Figure 12 was $t = 2.0$ s.

Length of the Front as a Function of Normalized Time

Figure 13 shows the normalized length of the interface as a

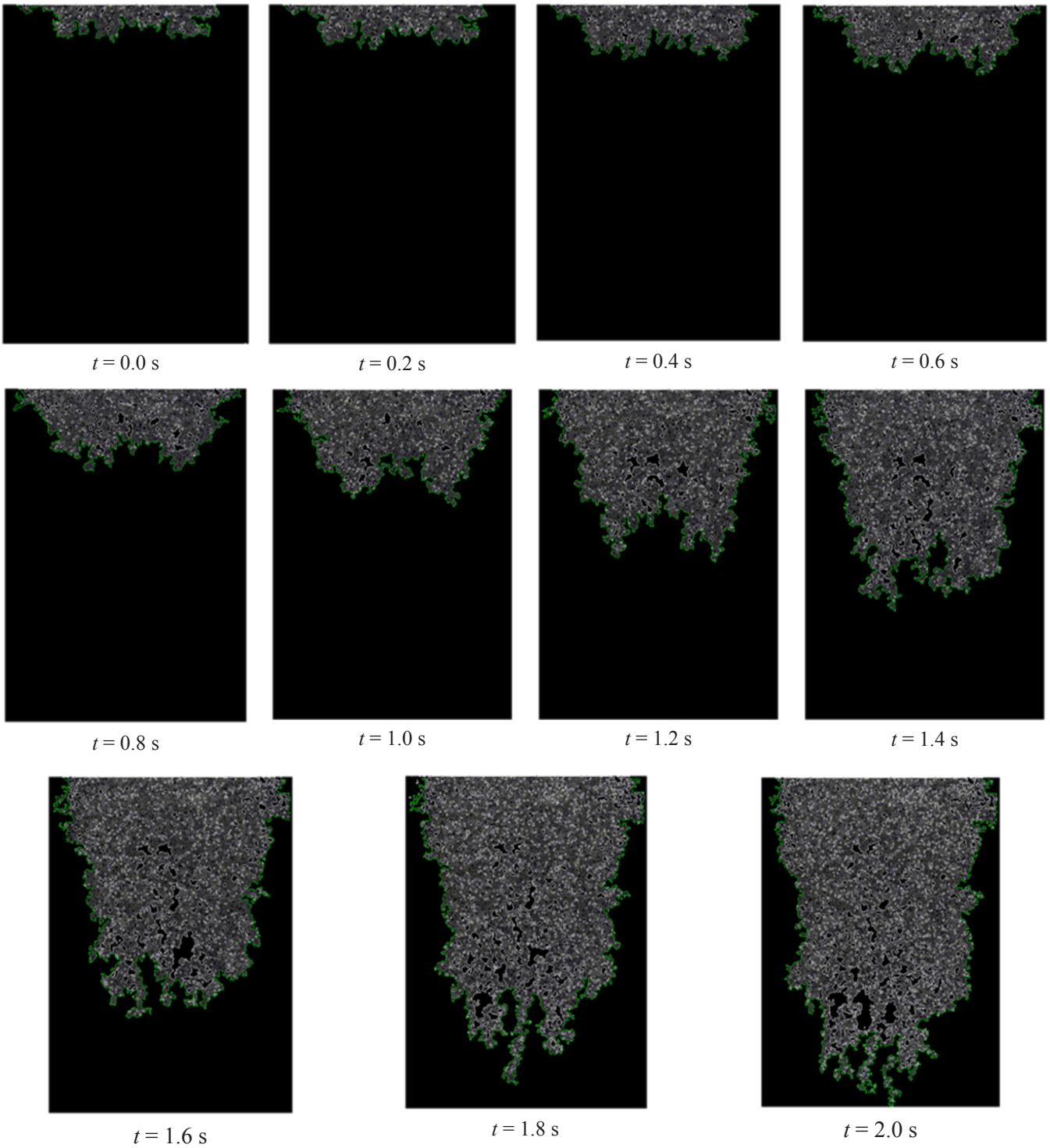

Figure 11. Profile of the interface for the fast flow during the drainage of the cell.

function of normalized time; the time for each curve is displayed in the upper left box of the figure. Figure 13 shows that the largest normalized length (i.e. 15.3) corresponds to the drainage that had the shorter duration (t = 0.9 s), while the smallest measured normalized length (i.e. 9.7) corresponds to the drainage of larger duration (t = 2.0 s); this indicates that the length of the interface can reach a value of up to 15 times the width of the cell.

Fractal Dimension

As for the slow flow case, the method used to calculate the fractal dimension of the fast flow was *Box Counting*. Figure 14 shows the variation of the fractal dimension as a function of normalized time; the duration of each curve (drainage) is shown in the upper left box. In this figure it is possible to observe that the fractal dimension is $FD = 1.172 \pm 0.07$.

Bribiesca's Discrete Compactness for the Fast Flow

Figure 15 shows the variation of the discrete compactness of three drainages with respect to normalized time based on estimating the contact perimeter. In Figure 15(a) it can be observed that at the beginning (t = 0 s) the three drainages have almost the same discrete compactness (40000), nevertheless, when the normalized time is T = 1 the difference between the larger and smaller value of the discrete compactness is 89200, that is, the discrete compactness when the normalized time is T = 1 for the drainage of longer duration (t = 2.0 s) is 1.2 times larger than the discrete compactness of the drainage of shorter duration (t = 0.9 s).

Figure 15(b) shows the normalized discrete compactness [Bribiesca (1997)]. In this figure the normalized discrete compactness can be observed to fluctuate between the values $0.942 \leq C_{DN} \leq 0.982$, these values represent the similarity between the interfaces for the fast flow case. In this figure it is possible to appreciate that the similarity between the interfaces grows as time increases ($0 \leq T \leq 0.8$), however, the similarity between the interfaces decreases for normalized times greater than $T > 0.8$.

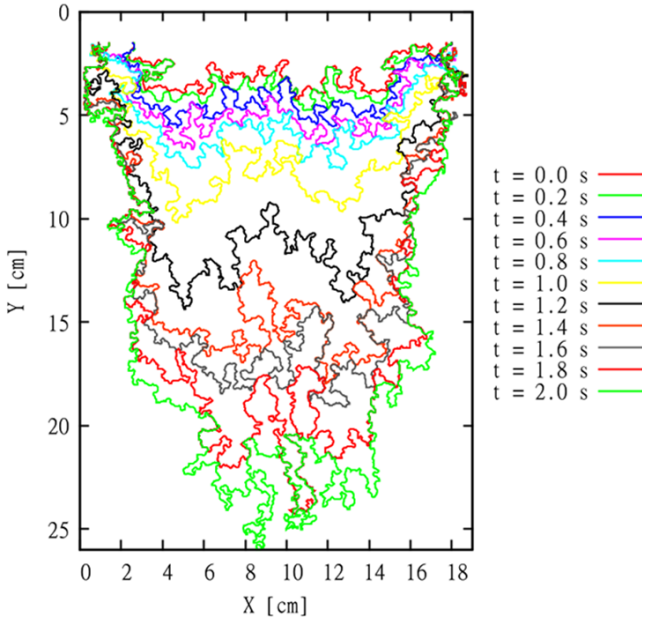

Figure 12. Sequence of the interface for the fast flow for different times of the drainage.

Conclusions

In this research several experiments for the drainage of a porous medium were carried out; the porous medium was prepared with glass beads of 1 mm in diameter and the porous medium was quasi two-dimensional. The results presented in this work indicate that it was possible to calculate very accurately the number of spheres contained in the porous medium, as well as the position of the centroid of each of them; this allowed carrying out a good characterization of the porous medium. The results show that the interface curves are not mathematical functions, due to this, it was necessary to resort to unconventional mathematical methods, such as the fractal dimension method and Bribiesca's discrete compactness method to analyze the cases of slow and fast flow.

The geometrical analysis showed the development of the interface curve between the water-air when the Hele-Shaw cell is drained slowly and it was also possible to measure the variation in the size of each of the interfaces, therefore, it was possible to determine that the normalized length of the interface for the slow flow ranges between the values of 1.2 to 1.4. Similarly, the fractal dimension for the slow flow was determined to be: $FD = 1.075 \pm 0.063$.

The method proposed by Bribiesca [Bribiesca (1997)] allowed determining the variation of the interface width; moreover, the normalized discrete compactness allowed knowing the similarity between the interfaces. It was found that the normalized discrete compactness lie in the range $0.925 \leq C_{DN} \leq 0.971$.

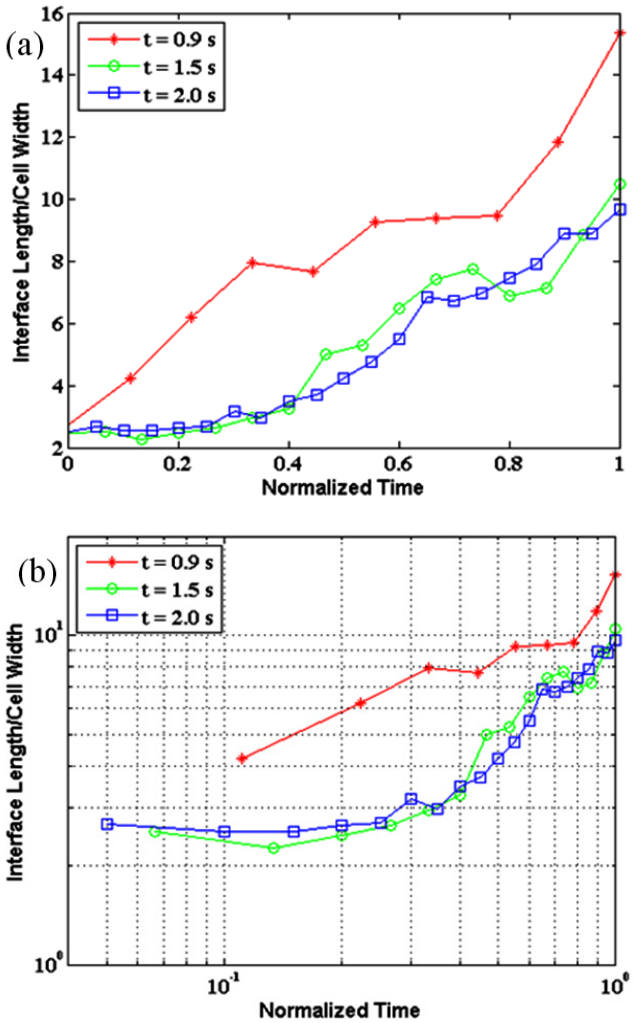

Figure 13. Normalized length of the interface as a function of normalized time for the fast flow. (a) Cartesian coordinates, and (b) log-log coordinates.

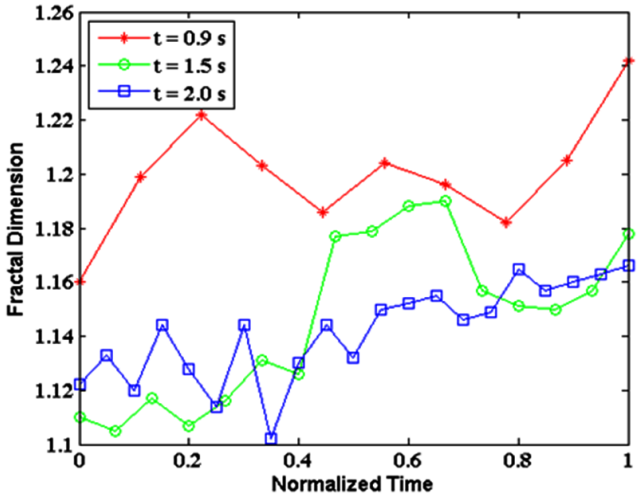

Figure 14. Fractal dimension with respect to normalized time for the fast flow interface.

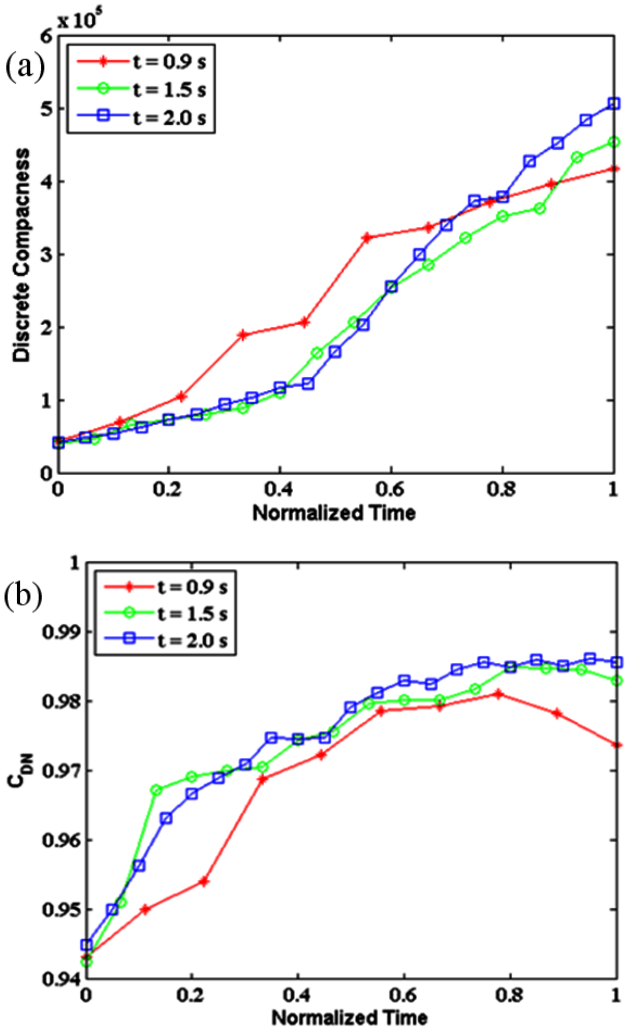

Figure 15. Discrete compactness for the fast flow using the contact perimeter. (a) Discrete compactness with regards to normalized time, and (b) normalized discrete compactness with regards to normalized time.

The geometrical analysis of the draining of the cell allowed observing that the interfaces of the fast flow are very different from the interfaces of the slow flow; also, it was possible to observe that the interfaces of the fast flow are more corrugated and wider. For the fast flow it was possible to determine that the length of the interface ranges from 2 to 16 times the cell width. Also, the fractal dimension calculated for the fast flow was $FD = 1.17 \pm 0.07$. Finally, the normalized discrete compactness showed that the similarity of the interfaces increases with time.

Flow in a porous medium is a complex scientific problem of great technological importance. The main contribution of the present work is the understanding of drainage through a porous medium at low and high velocities; this is essential knowledge to successfully perform the ecological rescue of soils contaminated by the oil industry, as well as for secondary recovery of oil, amongst other applications.

References

J. Bear, *Dynamics of fluids in porous media* (American Elsevier, New York, 1972).

G.M. Homsy, *Viscous fingering in porous media*, Annual Review of Fluid Mechanics, Volume 19, pp. 271-311 (1987).

H.A. Tchelepi and F.M. Orr, *Interaction of viscous fingering, permeability heterogeneity, and gravity segregation in three dimensions*, Society of Petroleum Engineers, Reservoir Engineering, Volume 9, Number 4, pp. 266-271 (1994).

D.G. Avraam and A.C. Payatakes, *Flow regimes and relative permeabilities during steady-state two-phase flow in porous media*, Journal of Fluid Mechanics, Volume 293, pp. 207-236 (1995).

R. Lenormand&C. Zarcone, *Invasion percolation in an etched network: measurement of a fractal dimension*. Physical Review Letters, Volume 54(20), pp. 2226–2229 (1985).

W.J. Da Sle, D.S. Guo, *Assessment of vertical hydrocarbon miscible flood in the West perm Nisku D Reef*. Society of Petroleum Engineers, Reservoir Engineering. Volume 5(2), pp. 147–154 (1990).

J. Hagoort, *Oil recovery by gravity drainage*. Society of Petroleum Engineers Journal, Volume 20(3), pp. 139–150 (1980).

K.J. Måløy, J. Feder, T. Jøssang, *Viscous fingering fractals in porous media*. Physical Review Letters. Volume 55, pp. 2688–2691 (1985).

A. Birovljev, L. Furuberg, J. Feder, T. Jøssang, K.J. Måløy, A. Aharony, *Gravity invasion percolation in 2 dimensions—experiment and simulation*. Physical Review Letters, Volume 67(5), pp. 584–587 (1991).

K.J. Måløy, L. Furuberg, J. Feder, T. Jøssang, *Dynamics of slow drainage in porous-media*. Physical Review Letters, Volume 68(14), pp. 2161–2164 (1992).

O.I. Frette, K.J. Maløy, J. Schmittbuhl, A. Hansen, *Immiscible displacement of viscosity-matched fluids in two-dimensional porous media*. Phys. Rev. E 55(3), 2969–2975 (1997).

R. Lenormand and C. Zarcone, *Capillary fingering: percolation and fractal dimension*, Transport in Porous Media Volume 4(6), pp. 599-612 (1989).

E. Aker, K.J. Måløy and A. Hansen, *Viscous stabilization of 2D drainage displacements with trapping*, Physical Review Letters, Volume 84(20), pp. 4589-4592 (2000).

J.-D. Chen and D. Wilkinson, *Pore-scale viscous fingering in porous media*, Physical Review Letters, Volume 55(18), pp. 1892-1895 (1985).

J. Nittman, *Fractal viscous fingering: Experiments and models*, Physica A: Statistical Mechanics and its Applications, Volume 140, 124-133 (1986).

T.A. Witten and L.M. Sander, *Diffusion-limited aggregation, a kinetic critical phenomenon*, Physical Review Letters, Volume 47(19), pp. 1400-1403 (1981).

T.A. Witten and L.M. Sander, *Diffusion-limited aggregation*, Physical Review B, Volume 27(9), pp. 5686-5697 (1983).

P. Meakin, *Diffusion-controlled cluster formation in 2—6-dimensional space*, Physical Review A, Volume 27(3), pp. 1495-1507 (1983).

L. Paterson, *Diffusion-Limited Aggregation and Two-Fluid Displacements in Porous Media*, Physical Review Letters, Volume 52(18), pp. 1621-1624 (1984).

E.L. Hinrichsen, K. J. MåLøY, J. Feder and T. Jøssang. *Self-similarity and the structure of DLA and viscous fingering clusters*. Journal of Physics A, Volume 22(7), pp. L271-L277 (1989).

F.A.L. Dullien, *Two-phase flow in porous media*. Chemical Engineering & Technology, Volume 11(1), pp. 407–424 (1988).

D. Wilkinson, *Percolation model of immiscible displacement in the presence of buoyancy forces*, Physical Review A, Volume 30(1), pp. 520-531 (1984).

A. Birovljev, G. Wagner, P. Meakin, J. Feder, and T. Jøssang, *Migration and fragmentation of invasion percolation clusters in two-dimensional porous media*, Physical Review E, Volume 51(6), pp. 5911-5915 (1995).

G. Wagner, A. Birovljev, P. Meakin, J. Feder, and T. Jøssang, *Fragmentation and migration of invasion percolation clusters: Experiments and simulations*, Physical Review E, Volume 55(6), pp. 7015-7029 (1997).

P. G. Saffman and G. Taylor, *The penetration of a fluid into a porous medium or Hele-Shaw cell containing a more viscous liquid*, Proceedings of the Royal Society London A, Volume 245(1242), pp. 312-329 (1958).

A. Vedvik, G. Wagner, U. Oxaal, J. Feder, P. Meakin, and T. Jøssang, *Fragmentation transition for invasion percolation in hydraulic gradients*, Physical Review Letters, Volume 80(14), pp. 3065-3068 (1998).

D. Zhou and F.M.J. Orr, *The effects of gravity and viscous forces on residual non wetting-phase saturation*, In Situ, Volume 19(3), pp. 249-273 (1995).

V. Frette, J. Feder, T. Jøssang, and P. Meakin, *Bouyancydriven fluid migration in porous media*, Physical Review Letters, Volume 68(21), pp. 3164-3167 (1992).

P. Meakin, A. Birovljev, V. Frette, J. Feder, and T. Jøssang, *Gradient stabilized and destabilized invasion percolation*, Physica A: Statistical and Theoretical Physics, Volume 191, pp. 227-239 (1992).

G. Wagner, P. Meakin, J. Feder, T. Jøssang, *Buoyancy-driven invasion percolation with migration and fragmentation*, Physica A: Statistical Mechanics and its Applications, Volume 245, pp. 217-230 (1997).

W.B. Haines, *Studies in the physical properties of soil. V. The hysteresis effect in capillary properties and the modes of moisture distribution associated therewith*, Journal of Agricultural Science, Volume 20, pp. 97-116 (1930).

E. Bribiesca, *Measuring 2-D shape compactness using the contact perimeter*, Computers & Mathematics with Applications, Vol. 33(11), pp. 1-9 (1997).